Journal of Hazardous Materials 268 (2014) 246–255

Contents lists available at ScienceDirect

Journal of Hazardous Materials

journal homepage: www.elsevier.com/locate/jhazmat

Incidence of the core composition on the stability, the ROS production and the toxicity of CdSe quantum dots

Florence-Anaïs Kauffer[a,b], Christophe Merlin[b], Lavinia Balan[c], Raphaël Schneider[a,*]

[a] Université de Lorraine, Laboratoire Réactions et Génie des Procédés (LRGP), UMR 7274, CNRS, 1 rue Grandville, BP 20451, 54001 Nancy Cedex, France
[b] Université de Lorraine, Laboratoire de Chimie Physique et Microbiologie pour l'Environnement (LCPME), UMR 7564, CNRS, 15 Avenue du Charmois, 54500 Vandoeuvre-lès-Nancy, France
[c] Institut de Science des Matériaux de Mulhouse (IS2M), LRC 7228, 15 rue Jean Starcky, 68093 Mulhouse, France

HIGHLIGHTS

- Aqueous phase routes for the production of MSA-capped CdSe and alloyed CdSe(S) QDs were developed.
- Despite their higher content in cadmium, CdSe(S) QDs are less toxic than CdSe ones.
- Hydroxyl radical production is correlated to the photostability of the dots.
- The surface chemistry and the reactivity of QDs play a crucial role on their phototoxicity.

GRAPHICAL ABSTRACT

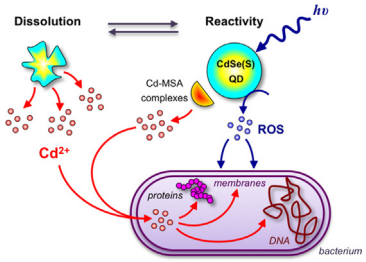

ARTICLE INFO

Article history:
Received 20 October 2013
Received in revised form 5 December 2013
Accepted 5 January 2014
Available online 24 January 2014

Keywords:
CdSe quantum dots
Aqueous synthesis
Photostability
Reactive oxygen species
Cytotoxicity

ABSTRACT

Mercaptosuccinic acid-capped CdSe and alloyed CdSe(S) QDs were prepared in aqueous solution at 100 and 170 °C, respectively. These dots were characterized by transmission electron microscopy (TEM), X-ray diffraction (XRD), and UV–vis and photoluminescence spectroscopies. The dots were found to be of similar size (ca. 2 nm) but differ in their composition and surface chemistry. The photostability of the QDs was found to correlate with their ability to produce reactive oxygen species (ROS) upon light activation. CdSe QDs produce hydroxyl radicals immediately after irradiation due to their modest photostability, while CdSe(S) QDs start to generate the hydroxyl radicals only once they start to be bleached (ca. 30 min). Cytotoxicity experiments conducted on *Escherichia coli* cells revealed that CdSe QDs were the more toxic despite being the least loaded in cadmium. In addition, consistent with ROS assays, the cytotoxicity of the CdSe QDs appeared light-dependent and is in accordance with a light-dependent oxidative stress observed with an *oxyR*-based whole cell biosensor. Our results demonstrate the crucial role played by nanoparticles synthesis process on their PL properties, their stability and their toxicity.

1. Introduction

Over the last fifteen years, quantum dots (QDs) have been increasingly used as biological imaging and labelling probes due to their unique optical properties, including broad absorption with narrow photoluminescence (PL) spectra, low photobleaching, high quantum yield, tunable emission from visible to infrared wavelengths, and better resistance to chemical degradation in comparison with organic fluorophores [1–4]. However, it has been discovered early in their development that the use of these nanomaterials poses serious concerns about toxicity and safety, especially because the most popular QDs like CdSe or CdTe contain highly toxic and carcinogenic elements. This raised an issue in the short term regarding the integrity of the studied biological material labelled using the dots, but also in the long term with the management of waste material. Studies utilizing CdSe

* Corresponding author. Tel.: +33 3 83 17 50 53; fax: +33 3 83 32 29 75.
E-mail address: raphael.schneider@univ-lorraine.fr (R. Schneider).

0304-3894/$ – see front matter © 2014 Elsevier B.V. All rights reserved.
http://dx.doi.org/10.1016/j.jhazmat.2014.01.029

core QDs have presented conflicting results. Early studies ascribed the toxicity to metal ions release in biological systems [5,6], with subsequent generation of reactive oxygen species (ROS) [7,8]. This cytotoxicity could be reduced by capping CdSe cores with a ZnS shell that prevents QD breakdown in solution [9,10], but there are concerns about cap loss and the subsequent toxicity of bare QDs and dissolved cadmium [5,11]. Other studies demonstrated that the capping ligand, and therefore the surface charge, could determine the cytotoxicity of QDs with positively charged QDs being more toxic than negative ones [12–14]. Some reports also highlighted the roles played by surface properties and/or the small size of these nanocrystals on QDs induced bio-effects [15,16]. In several instances, Cd-based QDs have been presented as more toxic to cells than their equivalent content in Cd^{2+} salts, implying that metal leaking is not the sole source of toxicity [16,17]. With this respect, another key factor affecting QDs-induced toxicity is their ability to generate ROS after light activation. Upon photoexcitation, the electrons can be scavenged by the adsorbed molecular oxygen to yield the superoxide radical anion ($O_2^{\bullet -}$), whereas the holes oxidize chemisorbed water to generate hydroxyl radicals ($^{\bullet}OH$). The nature/quality of the QD surface determines the number of trap states [18], which in turn affects electron-hole recombination and thus the charge transfer between photoexcited electrons and holes and adsorbed molecules. Bare CdSe [19] and CdTe [20] QDs, and even core/shell CdSe/ZnS QDs [21], are known to produce ROS under light irradiation but there are huge structural differences between these dots, leading to different level of reactivity, and it is therefore difficult to establish a general trend on the ability to produce ROS.

In fact, Cd^{2+} release and QDs reactivity, which depend on their physicochemical properties (size, core composition, surface chemistry, and redox properties), may be influenced by the QD-biological interactions, thereby necessitating a multimodal approach to evaluate QDs toxicity. At this point, it should be noted that because most toxicity studies were carried out independently, each one under specific experimental conditions, any comparison to identify a particular relationship between a QD structural features and a particular trend in its toxicity is quite impossible.

High quality CdSe QDs can be synthesized via the hot-injection approach conducted in coordinating solvents/ligands such as tri-n-octylphosphine (TOP), tri-n-octylphosphine oxide (TOPO), or oleic acid (OA) [22–24]. However, in order to meet the requirement of bioapplications, such hydrophobic QDs need to be transferred from the organic phase to aqueous solution. The exchange of the hydrophobic TOP, TOPO, or OA ligands with hydrophilic ones such as thioacids, and subsequent transfer of QDs from oil to aqueous solution can significantly reduce the PL quantum yield (PL QY) and the stability of the nanocrystals [25]. Direct synthesis of hydrophilic thiol-capped QDs in water is a valuable alternative to the organic phase synthesis and offers the following advantages: (1) it uses less toxic reagents, (2) it is cheaper and simpler, (3) it uses low temperatures to obtain QDs, and (4) the surface functionalization with water-soluble ligand occurs during the synthesis. However, the synthesis of QDs in water generally affords QDs with modest PL QYs (less than 10%) [26]. In recent years, much effort has therefore been devoted to improve the optical properties of aqueous-phase prepared QDs. We recently developed hydrothermal methods that enable the production of highly fluorescent and water-dispersible CdS [27], CdSe [28], and CdTe [29] QDs and this strategy was successfully extended to core/shell heterostructures.

This work describes the aqueous-phase synthesis, the characterization and the photostability of mercaptosuccinic acid (MSA)-capped CdSe and ternary alloyed CdSe(S) QDs. The ability of these dots to generate ROS in water was investigated and correlated with cytotoxicity studies on bacteria cells performed either in the dark or under visible light irradiation. The main differences between the two investigated QDs are their composition (CdSe vs. CdSe(S)) and their surface chemistries, while other properties that may affect cellular responses like surface ligand, charge and size are kept almost constant, and should therefore provide a direct comparison of the impact of the QD core material on toxicity towards bacteria cells.

2. Materials and methods

2.1. Synthesis of CdSe QDs

The full list of chemicals used in this work and the preparation of NaHSe [30] is described in the supplementary information. CdSe(S)@MSA and CdSe@MSA QDs were prepared by reaction between $CdCl_2{\cdot}2.5H_2O$ and NaHSe in the presence of MSA following the method described previously [31], with some modifications. Briefly, 15.4 mg of $CdCl_2{\cdot}2.5H_2O$ (67 μmol) and 10.5 mg of MSA (70 μmol) were dissolved in 39 mL and 26 mL of water, respectively. Both solutions were mixed and the pH was adjusted to 10 with 0.1 M NaOH. After 30 min of Ar-degassing, 320 μL of 0.05 M NaHSe solution were injected in the precursor solution. The solution turned yellow immediately. CdSe@MSA QDs were obtained by refluxing the solution for 5 min. CdSe(S)@MSA QDs were prepared by refluxing the solution for 20 min before transfer into a Teflon-lined stainless steel autoclave at 170 °C for 1 h. After cooling down, the reaction mixture was concentrated, and QDs were precipitated with *i*-PrOH. QDs were collected by centrifugation, washed 3 times with *i*-PrOH, and dried at room temperature under vacuum.

2.2. QDs characterization

All the optical measurements were performed at room temperature. Absorption spectra were recorded on a Thermo Scientific Evolution 220 UV–visible spectrophotometer. PL spectra were recorded on a Horiba Fluorolog 3 F222 Jobin Yvon spectrofluorimeter. The PL QY values were determined from the following equation:

$$QY_{sample} = \left(\frac{F_{sample}}{F_{ref}}\right)\left(\frac{A_{ref}}{A_{sample}}\right)\left(\frac{n^2_{sample}}{n^2_{ref}}\right)(QY_{ref}),$$

where F, A and n are the measured fluorescence, the absorbance at the excitation wavelength, and the refractive index of the solvent, respectively. Fluorescence emission spectra were spectrally corrected and the PL QYs were determined relative to Rose Bengal in ethanol (QY = 11%) [32]. QDs concentration was estimated from the reported extinction coefficient per mole of particles (ε) by using the Beer–Lambert's law [33]. Photostability of QDs was evaluated by irradiating 2 mL of 5 μM dispersions with a Hg–Xe lamp (P = 350 mW).

TEM experiments were conducted on a Philips CM20 instrument with a LaB6 cathode operating at 200 kV. XRD analyses were conducted on a Panalytical X'pert Pro MPD diffractometer by using a Cu Kα radiation. Dynamic light scattering (DLS) and zeta potential measurements were performed at 25 °C using a Zetasizer NanoZS ZEN3600 Malvern instrument using an He–Ne laser (4×10^{-3} W) at a wavelength of 633 nm. The hydrodynamic diameter (d_H) and the size distribution of QDs dispersions were obtained by using the Stokes–Einstein relation. A VARIAN 720-ES inductively coupled plasma-optical emission spectrometer (ICP-OES) was used for multielemental analyses.

2.3. Cytotoxicity assays

Growth inhibition tests were carried out on *Escherichia coli* MG1655 in one-tenth diluted LB medium (1/10th LB) at 30 °C

under agitation (160 rpm). Exponentially growing cultures of *E. coli* MG1655 (OD_{600} = 0.1) were one-fourth diluted in pre-warmed 1/10th LB medium supplemented with the desired concentration of QDs and the OD_{600} was measured at intervals. A growth control without QDs supplement was performed in parallel. For each growth condition, the generation times of exponential growing cultures (T_g) were calculated from the slope of an exponential trend curve. Growth experiments carried out either in the dark or under the illumination (1250 lx) of a full spectrum neon lighting (T8 Solar Color JBL).

2.4. Quantification of bioavailable Cd^{2+} produced by CdSe and CdSe(S) QDs

Bioavailable Cd^{2+} originating from QDs dissolution was quantified using the whole cell biosensor *Cupriavidus metallidurans* AE1433, a genetically engineered bacteria emitting light when sensing bioavailable Cd^{2+} [37]. The full synthetic protocol used is described in the supplementary information. For each series, luminescence induction factors (IF) were plotted against $CdCl_2$ (standard curve) or QD (test) concentrations, where equations were obtained from linear regressions of the non-toxic part of the curve: equation #1 ($CdCl_2$ standard curve): IF = a [Cd^{2+}] + 1 and equation #2 (QD test curve): IF = b [QD] + 1, with "a" and "b" corresponding to the slopes of both curves. Thus, for a same IF, a [Cd^{2+}] + 1 = b [QD] + 1 $\Leftrightarrow$ [Cd^{2+}]/[QD] = b/a, and knowing the estimated amount of Cd atoms per QD (75 for CdSe@MSA and 184 for CdSe(S)@MSA, respectively) it is then possible to calculate the relative amount of Cd that leaked from the QDs.

2.5. ROS evaluation

2.5.1. Chemical detection

2.5.1.1. NBT assays. The production of $O_2^{\bullet -}$ radicals was estimated using the nitroblue tetrazolium (NBT) assay [34]. NBT assay is based on spectrophotometric measurements quantifying the reduction of yellowish NBT into purple formazan derivatives. This reduction into mono- and diformazan derivatives results in an increase of absorbance between 450 and 700 nm. Typically, a solution of QDs (2.5 μM) and NBT (200 μM) was prepared in a 1:1 water/DMSO mixture (2 mL) and was irradiated by a Hg–Xe lamp (P = 50 mW) for various times. The absorbance spectra were recorded to quantify formazan derivatives formed. Reference samples were (i) NBT irradiated in the absence of QDs and (ii) NBT + QDs without light activation.

2.5.1.2. DST assays. The production of hydroxyl radicals ($^{\bullet}$OH) by QDs was estimated using disodium terephthalate (DST), which turns into fluorescent hydroxyterephthalate (λ_{em} = 428 nm) upon reaction with $^{\bullet}$OH radicals. Briefly, 1 mL of QDs water dispersion (10 μM, 10 nmol) was mixed with 1 mL of DST (1 mM in water, 1 μmol) before being irradiated (P = 350 mW). The mixture was treated with 1 mL of 1 M NaOH and incubated for 50 min at r.t. before filtration on 0.2 μm polyvinylidene fluoride Acrodisc Syringe Filter. The PL spectra were recorded to quantify 2-OH-DST formed. A 2-OH-DST calibration curve was also constructed in order to convert fluorescence intensity measured in a molar concentration of hydroxyl radicals. Calculations were made considering a 1:1 stoichiometry for the reaction between DST and $^{\bullet}$OH. The conversion of DST into 2-OH-DST [35] was characterized by a 35% yield. 2-OH-DST used as reference was synthesized as described [36].

2.5.2. Detection of QD-generated oxidative stress

H_2O_2-generated oxidative stress was evaluated using the biosensor *E. coli* MG1655(pUA66::P_{oxyR}) resulting from the fusion of the H_2O_2-regulated *oxyR* promoter with the *gfp* reporter gene [38]. A full description of the use of the biosensor is provided in the supplementary information.

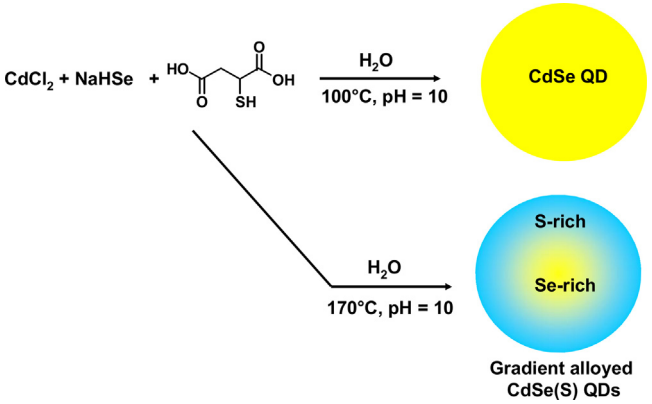

Fig. 1. Schematic illustration of the synthetic routes used for the preparation of CdSe@MSA and CdSe(S)@MSA QDs.

3. Results and discussion

3.1. Synthesis, size, shape, crystal structure and PL properties of CdSe and CdSe(S) nanocrystals

MSA-capped CdSe and CdSe(S) QDs were prepared by reaction of Cd-MSA complexes with NaHSe at pH = 10. Cadmium monomers react with selenide ions to form a CdSe core at low temperature (100 °C). At high temperature and under pressure (170 °C, hydrothermal synthesis), the excess cadmium monomers react with sulphide ions released from MSA to form CdS, which deposits onto the surface of CdSe resulting in alloyed CdSe(S) QDs (Fig. 1) [28]. The XRD patterns of CdSe@MSA and CdSe(S)@MPA QDs prepared are shown in Fig. 2, together with those of bulk CdSe and CdS for reference. Broadening of the diffraction peaks indicates the small size of the obtained nanocrystals. For CdSe QDs, the diffraction features appearing at 25.98° and 43.70° correspond to the (1 1 1) and (2 2 0) planes for cubic CdSe (JCPDS Card No 19.191). For CdSe(S) QDs, a third peak corresponding to the (3 1 1) plane appears at 50.76°, indicating the higher crystallinity of nanocrystals produced, and (1 1 1) and (2 2 0) diffraction peaks shift to the diffraction of large Bragg angles, which is indicative of a decrease in the lattice parameters. This originates from an increase in S content into the CdSe lattice and shows the formation of alloyed CdSe(S) QDs under hydrothermal conditions.

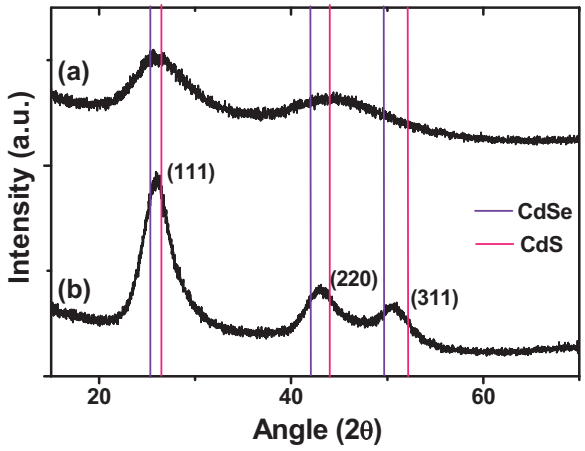

Fig. 2. X-ray diffraction patterns of (a) CdSe and (b) CdSe(S) QDs. The standard patterns of bulk CdSe and CdS are present as references.

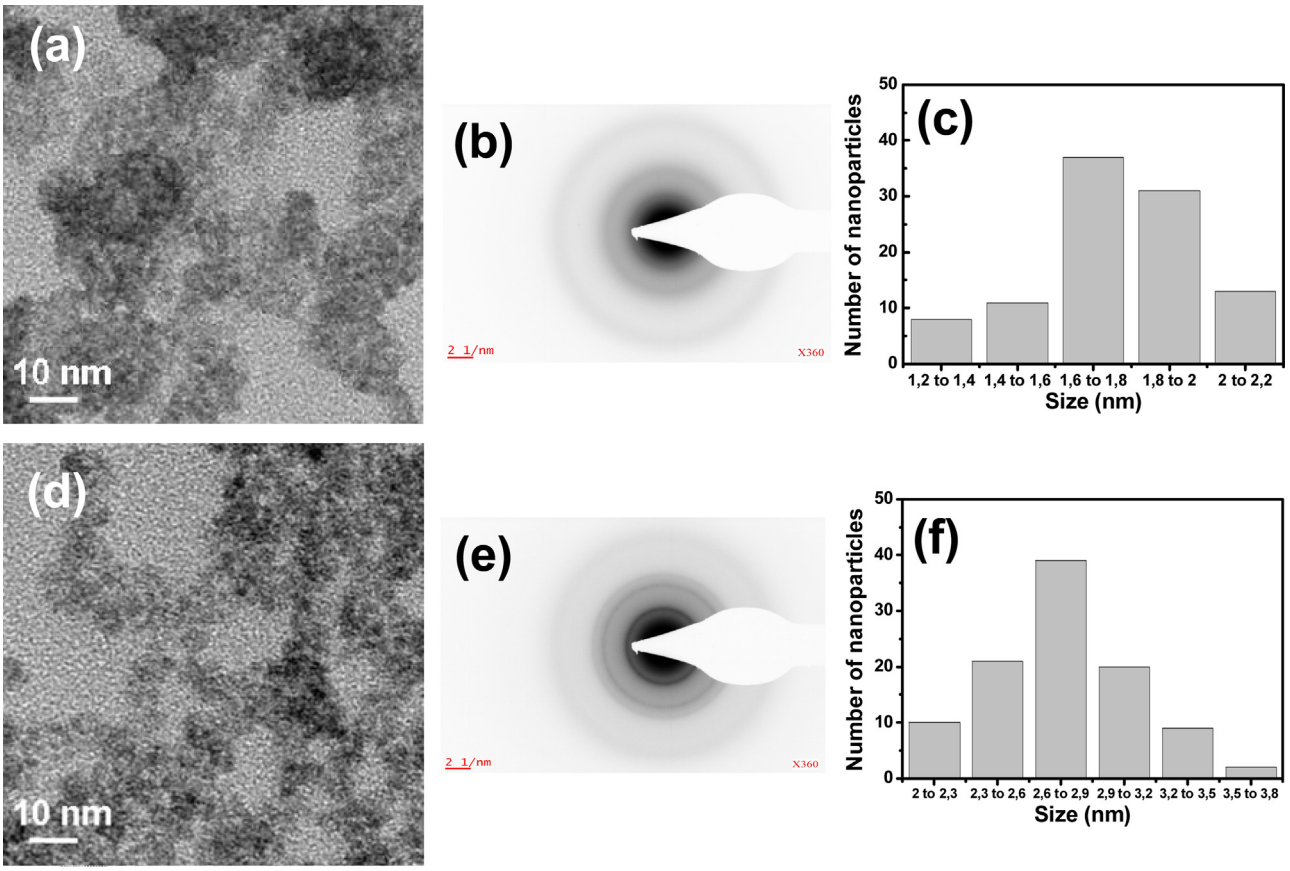

Fig. 3. Representative TEM images of (a) CdSe and (d) CdSe(S) QDs. (b) and (e) are the corresponding electron diffraction patterns and (c) and (f) the histograms of particle size distributions.

Fig. 3a and d shows the typical TEM images of CdSe and CdSe(S) QDs, respectively. QDs exhibit good monodispersity and nearly spherical/ellipsoidal shape with a narrow size distribution (Fig. 3c and f). The average crystalline sizes of CdSe and CdSe(S) QDs were estimated to be 1.8 ± 0.2 and 2.7 ± 0.3 nm, respectively. The selected area electron diffraction (SAED, Fig. 3b and e) clearly gives three diffraction rings of (1 1 1), (2 2 0) and (3 1 1) planes from inner to the outer, which confirm the cubic phase CdSe and symmetry spatial group *F*43*m*. The average hydrodynamic sizes determined from DLS data were respectively of 4.3 ± 0.7 and 4.5 ± 0.8 nm for MSA-stabilized CdSe and CdSe(S) QDs, showing that the nanoparticles dispersed well in water. The electrical potential, referred to as the zeta ζ potential, which controls the colloidal stability and interparticle interactions, was also measured. At pH = 7.0, the ζ values measured for CdSe@MSA (-41 ± 5 mV) and CdSe(S)@MSA (-60 ± 5 mV) QDs confirmed the presence of negative charges on the surface of QDs, due to the carboxylate end groups of the MSA ligand.

Fig. 4 shows UV–vis absorption and PL spectra of CdSe and CdSe(S) QDs, respectively. The sharp excitonic absorption peaks located at 440 and 528 nm for CdSe and CdSe(S), respectively, indicate that the particles size and shape are nearly uniform, which is in good agreement with Fig. 3. For CdSe@MSA nanocrystals, no excitonic PL emission was observed and the dots exhibited only trap states emission centred at 612 nm (Fig. 4a). CdSe(S)@MSA QDs exhibit higher spectral quality as compared to that of CdSe QDs. The PL emission is sharp and symmetric, and the full-width at half-maximum was less than 50 nm (Fig. 4b). This spectral feature can be ascribed to the high crystallinity of CdSe(S) QDs. It is worth to mention that the low energy trap state luminescence peak was also observed during the preparation of CdSe(S) after short reaction times (30 min), but this peak became gradually weaker upon extending reaction time and finally disappeared after 1 h reaction. This can be explained by the alloying and the growth of the CdS shell which can effectively reduce the non-radiative trap and thus increase the band edge emission. Finally, PL QYs of CdSe and CdSe(S) QDs were found to be 14 and 22%, respectively.

3.2. Photostability of CdSe@MSA and CdSe(S)@MSA

Besides the PL QY enhancement, the alloying also leads to improvement in photostability. Fig. 5 shows the time–course curves of absorption and PL intensity of CdSe and CdSe(S) QDs under a continuous excitation with a Hg–Xe lamp ($P = 350$ mW) for 1.5 h. The irradiation of CdSe QDs capped by thioacids like MSA is well-known to promote oxidation of unsaturated Se atoms. In the meanwhile, the thioacid is oxidized into disulphide and detaches from QD surface, resulting in photobleaching and aggregation [28,29,39,40]. For both QDs, the PL intensity increased the first minutes of irradiation (10 min for CdSe and 30 min for CdSe(S)) because surface traps were gradually eliminated by photocorrosion which generates core/shell CdSe/CdS or CdSe(S)/CdS QDs (Fig. 5b and d). After 20 min of irradiation, the PL intensity of CdSe QDs returned to its initial value, then dropped rapidly, and was reduced to ca. 20% after 30 min, and finally disappeared after 1 h. As can also be observed on absorption spectra, the decomposition/detachment of the MSA ligand reduces QDs dispersibility in water, and leads to aggregation and precipitation of the nanocrystals. Alloyed CdSe(S) QDs possess much better performance under the same experimental conditions. Notably, there was nearly no photobleaching/aggregation observed for these dots until 45 min of irradiation. Aggregates appeared in solution only after 1 h and the

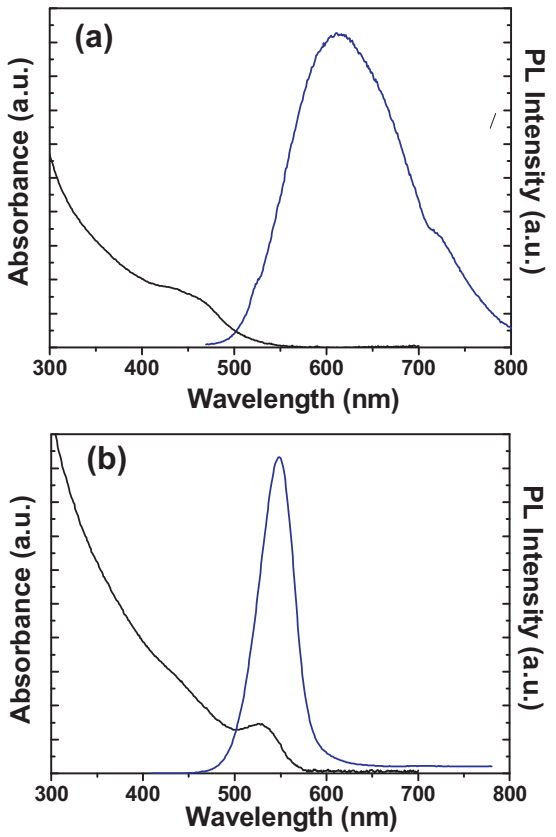

Fig. 4. UV–vis absorption spectra (black) and fluorescence spectra (blue) of (a) CdSe@MSA and (b) CdSe(S)@MSA QDs. (For interpretation of the references to colour in this figure legend, the reader is referred to the web version of the article.)

PL intensity gradually decreased (65%) and ultimately went down to ca. 25% of the original after 1.5 h.

3.3. Cytotoxicity studies

3.3.1. Cadmium releasable by CdSe@MSA and CdSe(S)@MSA QDs

The toxicity of Cd-based QDs has often been attributed, at least partially, to the release of Cd^{2+} ions [5,6]. Bioavailable Cd^{2+} ions released from both QDs was quantified using the whole cell biosensor *C. metallidurans* AE1433. The recombinant *C. metallidurans* AE1433 contains the lux*CDABE* bioluminescent genes downstream of a Cd^{2+}-responding promoter. The response of the biosensor to Cd^{2+} was expressed as an increase of luminescence compared to the background values without metal (induction factor). Cd^{2+} from $CdCl_2$ was considered 100% bioavailable and used as standard (Fig. 6). As shown in Fig. 6a, the biosensor provided a linear response for Cd^{2+} concentrations ranging from 0 to 2000 nM, indicating its usability for the corresponding range of induction factors (IF from 1 to 10). Exposure of AE1433 to known concentrations of CdSe@MSA and CdSe(S)@MSA QDs, provided linear responses of the biosensor until 5 and 10 nM of nanoparticles, respectively (Fig. 6b and c). Calculations made within this range of QD concentrations indicated a surprisingly high leakage of Cd^{2+}, going beyond the theoretical complete dissolution of the QD, with an average of $110 \pm 10\%$ and $123 \pm 9\%$ (3 repeats each) of the estimated Cd content for CdSe@MSA and CdSe(S)@MSA QDs, respectively.

Assuming a spherical geometry, average diameters of 2.0 and 2.7 nm for CdSe and CdSe(S) QDs (based on the molar extinction coefficient ε [33]) represent ca. 19 and 46 CdSe structural units in each nanocrystal of cubic structure using a theoretical lattice parameter a of 0.608 nm (JCPDS Card No. 19.191). Thus, each CdSe and CdSe(S) QD should contain ca. 75 and 184 Cd atoms, respectively. ICP-MS analyses carried out on 5 μM QD dispersions confirmed that both contained more Cd^{2+} ions than anticipated,

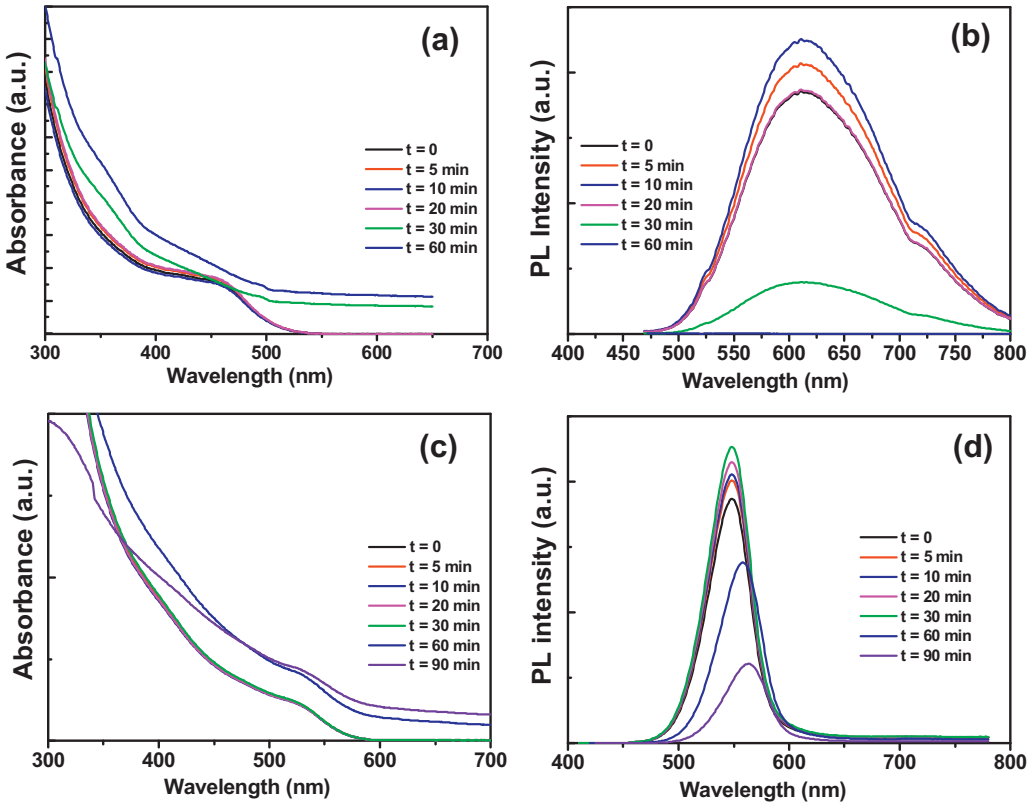

Fig. 5. Time evolutions of (a) and (c) absorption spectra and (b) and (d) PL emission spectra of CdSe(S) and CdSe(S) QDs, respectively, during irradiation with a Hg–Xe lamp.

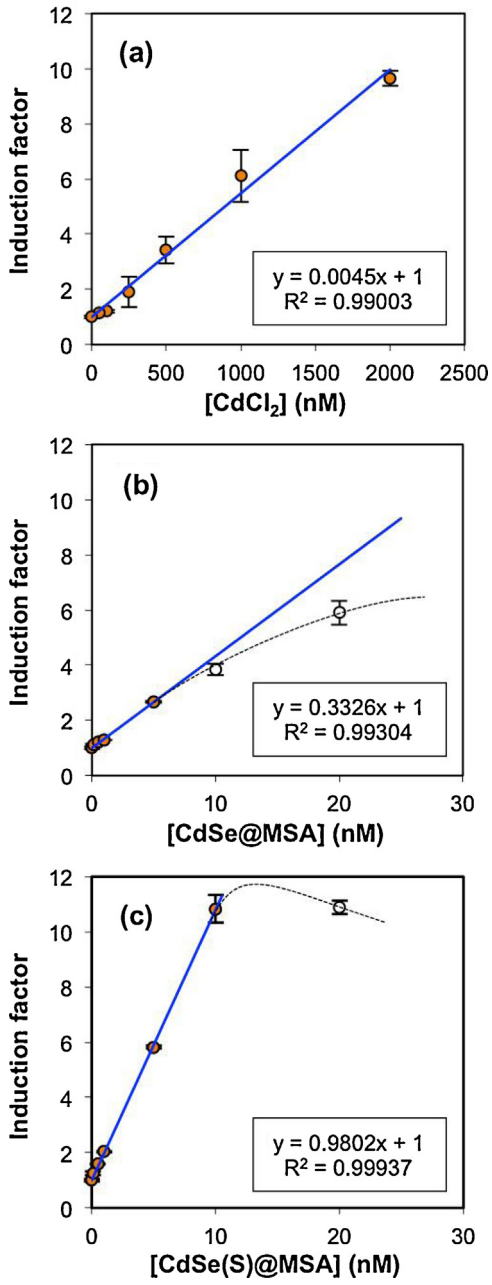

Fig. 6. Bioavailable Cd^{2+} released by CdSe@MSA and CdSe(S)@MSA QDs measured with biosensor AE1433. (a) Calibration curve used to determine the correspondence between the induction of bioluminescence and the concentration of bioavailable Cd^{2+}. (b) and (c) Bioluminescence induced by CdSe@MSA and CdSe(S)@MSA QDs, respectively. The equations obtained from linear fits were used to determine the amount of Cd^{2+} released by each QD. The experiment, carried out in triplicate gave an average Cd^{2+} release of 110 ± 10% and 123 ± 9% with respect to the expected Cd-content of CdSe@MSA and CdSe(S)@MSA QDs, respectively (as estimated using the absorption spectra).

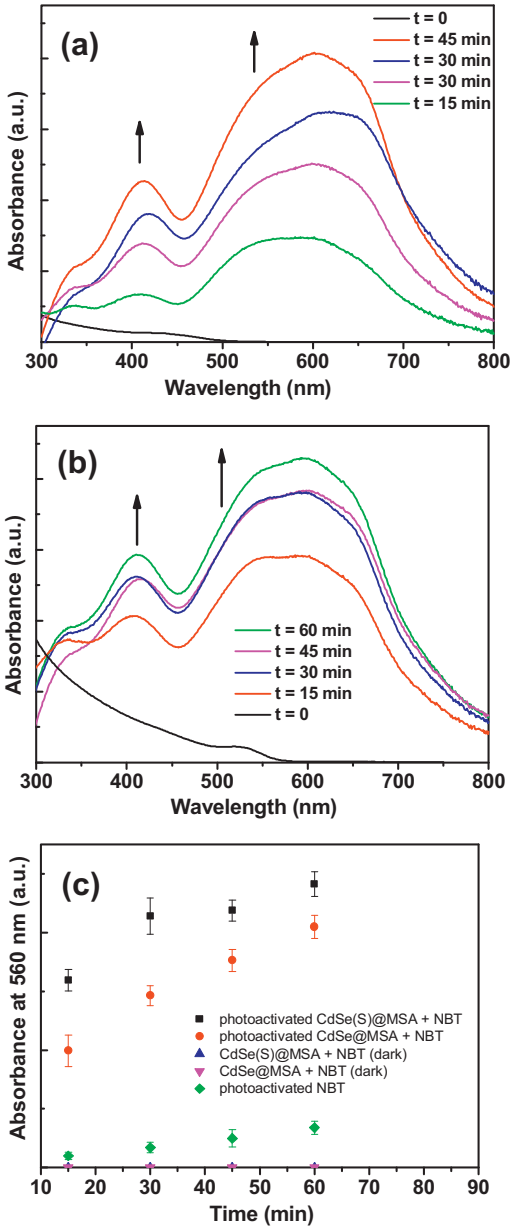

Fig. 7. Typical time evolutions of the absorption spectra of mono- and diformazan (i.e. $O_2^{\bullet-}$ formation) upon irradiation of NBT in O_2-purged solutions with (a) CdSe and (b) CdSe(S) QDs (black lines), and (c) temporal evolution of the absorption at 560 nm of NBT-QD and control experiments.

with a 27% excess for CdSe@MSA (i.e. 104 μM of Cd in addition to the 375 μM expected) and a 66% excess for CdSe(S)@MSA (i.e. 612 μM of Cd in addition to the 920 μM expected). Although these results do not fully explain the high levels of bioavailable Cd^{2+} ions observed, they suggest that Cd released after dispersion does not solely come from the nanoparticles dissolution, but may also originate from Cd–MSA complexes adsorbed at the surface of the dots [41] and co-purified with the QDs, thus rendering more complex our current perception of QDs toxicity. Finally, these results also show that the CdSe QDs dispersion carries ca. 3 times less cadmium than CdSe(S) one, which should be put in perspective while discussing the toxicity of these dots.

3.3.2. *Superoxide radical production by CdSe@MSA and CdSe(S)@MSA QDs*

The production of superoxide $O_2^{\bullet-}$ radicals by CdSe@MSA and CdSe(S)@MSA QDs was evaluated with a scavenging assay based on their ability to reduce nitroblue tetrazolium chloride (NBT) in a 1:1 water/DMSO mixture into dark blue formazan derivatives [34]. The reduction of NBT, principally into monoformazan, and to a lesser extent into diformazan derivatives, results in an increase of the absorbance in the 450–700 nm range (Fig. 7). Typical UV–vis absorption spectra recorded upon irradiation of NBT with CdSe and CdSe(S) QDs are provided in Fig. 7a and b, respectively, and the

evolutions of absorption at 560 nm are given in Fig. 7c. Experiments were conducted during various time of photoactivation in the presence of oxygen. As can be seen, the $O_2^{\bullet-}$ radical anion sensor showed a signal for both QDs (increase of the formazan derivatives optical density over time). CdSe(S) QDs generated slightly more $O_2^{\bullet-}$ radicals than CdSe and a plateau was reached for both dots after ca. 30 min irradiation. The concentrations of $O_2^{\bullet-}$ radicals after 60 min irradiation in O_2-saturated solutions were estimated using the molar extinction coefficient of monoformazan at 560 nm ($\varepsilon = 15{,}000\ M^{-1}\ cm^{-1}$) and found to be 273 ± 13 and $322 \pm 14\ \mu M$ for CdSe@MSA and CdSe(S)@MSA QDs, respectively. These values are in good accordance with those determined by Cooper et al. from aqueous dispersions of CdSe/ZnS QDs [21], but they remain weak compared to results obtained with metal oxide nanocrystals like ZnO which are well-known to be strong $O_2^{\bullet-}$ radicals producers [42]. Quite similar results to those described in Fig. 7 were obtained when QDs solutions were bubbled with nitrogen, further confirming the poor capability of CdSe and CdSe(S) QDs to generate $O_2^{\bullet-}$ radicals. Finally, control experiments conducted in the dark showed no reduction of NBT, thus confirming the photo-induced generation of $O_2^{\bullet-}$ radicals through electron transfer from CdSe and CdSe(S) to surrounding O_2 molecules.

3.3.3. *Photocatalytic generation of hydroxyl radical by CdSe@MSA and CdSe(S)@MSA QDs*

The formation of hydroxyl OH• radicals by photoreduction of oxygen upon irradiation with a lamp Hg–Xe lamp (200 mW) was monitored by trapping the radicals with disodium terephthalate (DST), a water-soluble and hydroxyl radical-specific probe. In this assay, non-fluorescent DST reacts with OH• radicals to form 2-OH-DST, which is a highly fluorescent anion emitting at ca. 430 nm in basic medium (see Fig. 8a and b for PL spectra as a time evolution) [43–46]. To this end, 1 mL of CdSe@MSA and CdSe(S)@MSA QDs (10 μM) was irradiated in the presence of 1 mL DST (1 mM) for various time. Samples were then treated with 1 mL NaOH (1 M), and the fluorescence intensity at 428 nm was measured. We first carried out studies where DST was incubated with QDs in the absence of light and adding or without adding NaOH to exclude the possibility of false positive due to dye interactions with the particle surface. In these control experiments, the fluorescence observed at 430 nm was found to be negligible, thus showing that OH• radicals formation was photo-induced. Due to the modest stability of CdSe QDs, their fluorescence was not observed on PL emission spectra upon treatment with NaOH (Fig. 8a). The PL emission of CdSe(S) QDs could be observed until 30 min of irradiation in the presence of DST (Fig. 8b) before their emission was fully bleached. During the first 25 min of irradiation, we found a significant signal from 2-OH-DST with CdSe but not with CdSe(S) QDs (Fig. 8). After ca. 30–40 min of irradiation, OH• radicals produced from CdSe@MSA QDs levelled off to a constant value. With CdSe(S) QDs, a rapid increase in 2-OH-DST production was observed only after 30 min irradiation, and a plateau was reached only after 1 h. Although the kinetics of the reactions differed, the final amounts of OH• radicals produced were very similar after the 75 min period (73 and 92 μM for CdSe and CdSe(S) QDs, respectively). Finally, we confirmed the QD-dependent generation of OH• radicals by adding mannitol, a well-known radical scavenger, in the reaction mixture during irradiation. In the presence of this compound, the oxidations of DST mediated by CdSe and CdSe(S) QDs were reduced by ca. 62 and 41%, respectively, compared to the experiments conducted without mannitol. At this point, it is also informative to relate the results of the DST assays to photostability experiments described in Fig. 5, although the intensity of the irradiation is not exactly the same. CdSe QDs were found to be of modest photostability, gradually decomposed during the irradiation and were quite totally bleached after ca. 30 min, which probably

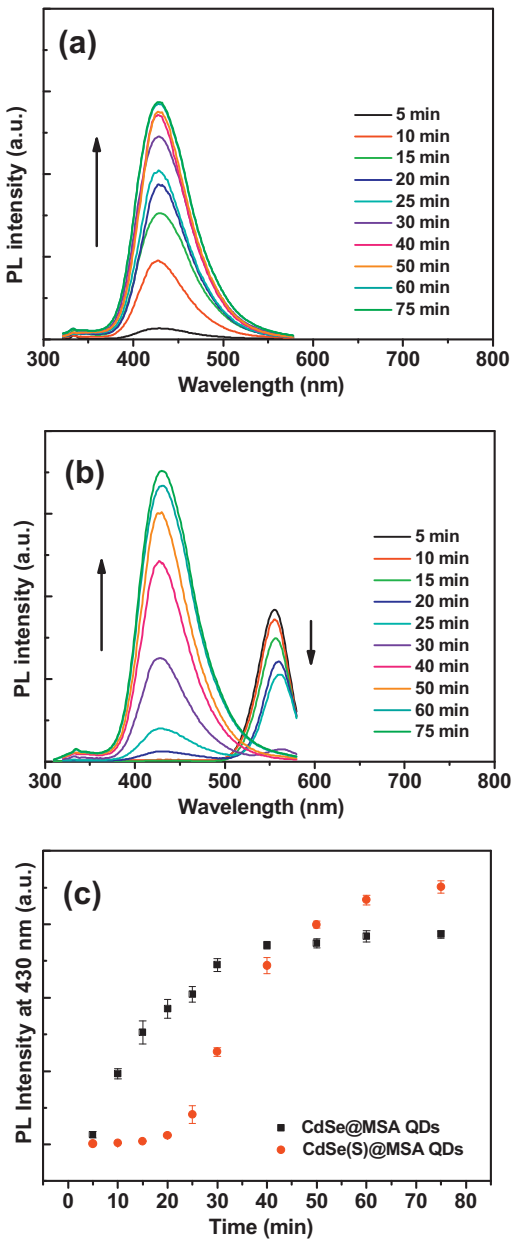

Fig. 8. Typical time evolutions of the PL emission spectra of 2-OH-DST (i.e. OH• formation) upon irradiation at λ = 365 nm of DST with (a) CdSe and (b) CdSe(S) QDs, and (c) variations of the PL intensity at 430 nm of 2-OH-DST.

corresponds to the plateau observed for OH• radicals production (Fig. 8c). Turning now to data recorded with CdSe(S)@MSA QDs, these dots were found to be of higher photostability and seem to generate OH• radicals only once the QDs start to degrade under photoirradiation.

3.3.4. *Cytotoxicity of CdSe@MSA and CdSe(S)@MSA QDs on E. coli bacterial cells*

The toxicity of both QDs was evaluated by exposing exponentially growing *E. coli* cells to various concentrations of QDs and monitoring growth kinetics. A first set of experiments carried out under illumination (1250 lx of full spectrum neon lighting) shows that the two QDs do not display the same level of toxicity (Fig. 9a). The toxicity of CdSe(S)@MSA QDs started to be visible at 1 μM with a dose-dependent increase of the generation time. CdSe@MSA QDs appeared more toxic with the first sign of toxicity already

(a) Generation times (Tg) obtained under light illumination

[QD] introduced (nM)	0	100	500	1000	2000	3000	4000
Generation time (min) for CdSe(S)@MSA QDs	44	45	45-43	47	51-53	56	69
Generation time (min) for CdSe@MSA QDs	44	51-49	54-55	57-59	66-65	70	no growth

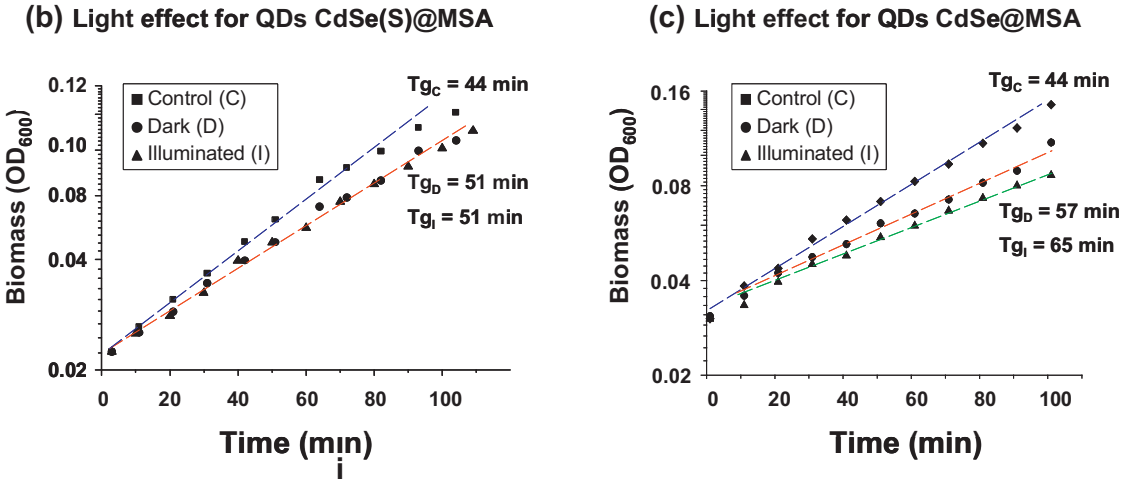

Fig. 9. Cytotoxicity of CdSe@MSA and CdSe(S)@MSA QDs. (a) Generation times (T_g) calculated for growth kinetics of *E. coli* MG1655 under illumination in presence of different concentrations of QDs. Growth was considered as inhibited when the generation time differs significantly form the control culture (44 ± 2 min; 21 repeats). Some tests were repeated twice for QDs concentrations presenting an effect. (b) and (c) Typical growth curves of *E. coli* MG1655 in absence (control) and in presence of 2 μM of either CdSe(S)@MSA or CdSe@MSA QDs. Duplicate experiments provided similar results: T_{gD} = 53 and 51 min, T_{gl} = 51 and 53 min for CdSe(S)@MSA, and T_{gD} = 57 and 55 min, T_{gl} = 66 and 65 min for CdSe(S)@MSA.

observable at 100 nM and a complete growth arrest at 4 μM. Such difference in QDs cytoxicity implies that it cannot only originate from the complete dissolution of the nanoparticle since the least toxic CdSe(S)@MSA QDs contain 3.2 times more Cd than CdSe@MSA QDs (vide supra). We next investigated the effect of suppressing light illumination at 2 μM of QDs, a concentration showing toxicity without preventing the cells from growing. Fig. 9b and c shows that the toxicity of CdSe(S)@MSA QDs remained unchanged regardless of the illumination conditions. In contrast, CdSe@MSA QDs were found to be less toxic in the darkness, thus indicating that a part of the toxicity was photo-induced.

If QDs toxicity is linked to ROS production, we hypothesized that *E. coli* cells should perceive an oxidative stress. An oxidative stress response biosensor, genetically modified to express the green fluorescent protein in the presence of H_2O_2, was exposed to both QDs at concentrations ranging from 1×10^{-12} to 1×10^{-8} M, under illumination or in the darkness. Fig. 10a shows that only a slight response was observed for CdSe(S)@MSA QDs with a maximum at 10^{-11} M and without real difference between the two illumination conditions. In contrast, with CdSe@MSA QDs, the biosensor did not respond in the dark, while a weak oxidative stress could be observed around 5×10^{-9} M (Fig. 10b). These results confirm that

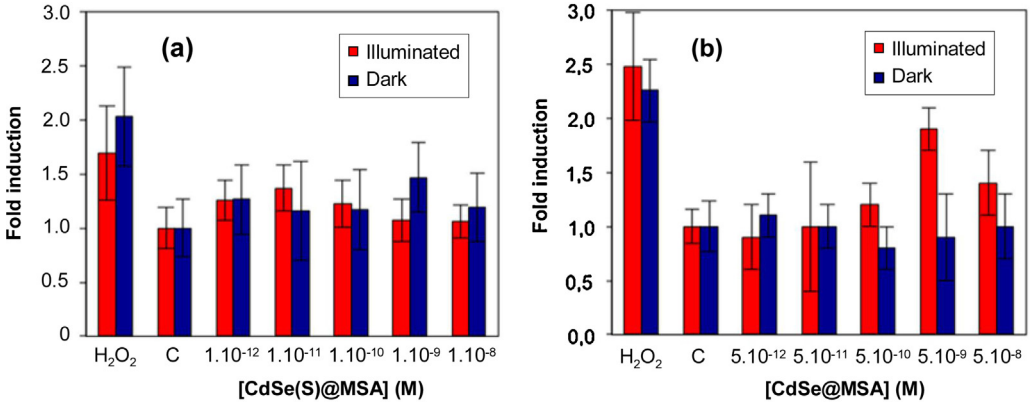

Fig. 10. H_2O_2-mediated oxidative stress response generated by CdSe@MSA (a) and CdSe(S)@MSA (b) QDs. H_2O_2: positive control providing a maximum response of biosensor MG1655(pUA66::*PoxyR*) for $[H_2O_2] = 5 \times 10^{-6}$ M; C: non-induced control.

each QD exert a different and specific oxidative stress towards *E. coli* cells, CdSe QDs being more reactive to illumination both in terms of cytotoxicity and hydroxyl radical production.

4. Conclusions

The mechanisms involved in the toxicity of the widely used Cd-based QDs are still subject to debate. This probably lies in the fact that the relative contributions of the two main sources of toxicity, i.e. Cd^{2+} ions release and ROS production, vary from one QD to another according to their synthesis methods, structures, or even simply through batch-to-batch variations. We demonstrated that two MSA-capped CdSe QDs of ca. 2 nm in diameter, but varying in their core compositions and surface chemistries, CdSe vs. CdSe(S), differ markedly in their toxicity. Although displaying a higher content of cadmium, the alloyed CdSe(S) QDs appeared less toxic than the CdSe ones.

CdSe and CdSe(S) QDs were analyzed for their light-induced ROS production, which were found to depend on the QD core material and on the irradiation time. CdSe QDs produced •OH radicals quite immediately after light activation, whereas CdSe(S) required extensive irradiation and partial photobleaching to generate an equivalent amount of radicals. The toxicity observed for CdSe QDs may be directly linked to •OH radicals produced. Without ruling out the importance of Cd^{2+} ions release, our results demonstrate that for such nanocrystals, the reactivity of the core plays a crucial role on QDs-induced phototoxicity. Our data also suggest that •OH radical formation, which is known among others to mediate membrane damage and subsequent cell death [46], can be circumvented or controlled by the choice of appropriate QD material and/or irradiation conditions. Our results should provide new insights into potential safety risks for the use of semiconductor nanoparticles in aerobic environment and under light exposition.

Acknowledgements

This work is supported by the Agence Nationale pour la Recherche (ANR CESA 2011, project NanoZnOTox). We thank Ghouti Medjahdi (IJL, Université de Lorraine) and Hélène Poirot (LRGP, Université de Lorraine) for XRD and ICP-MS analyses, respectively, and are grateful to Hélène Guilloteau (LCPME, Université de Lorraine) for technical support. We thank Dr. Serge Corbel (LRGP, Université de Lorraine) for facilitating photostability experiments.

Appendix A. Supplementary data

Supplementary data associated with this article can be found, in the online version, at http://dx.doi.org/10.1016/j.jhazmat.2014.01.029.

References

[1] I.L. Medintz, H.T. Uyeda, E.R. Goldman, H. Mattoussi, Quantum dot bioconjugates for imaging, labelling and sensing, Nat. Mater. 4 (2005) 435–446.
[2] W.A. Hild, M. Breunig, A. Goepferich, Quantum dots—nano-sized probes for the exploration of cellular and intracellular targeting, Eur. J. Pharm. Biopharm. 68 (2008) 153–168.
[3] A. Rogach, Semiconductor Nanocrystal Quantum Dots: Synthesis, Assembly, Spectroscopy and Applications, Springer Verlag, Vienna, Austria, 2008.
[4] X. Michalet, F.F. Pinaud, L.A. Bentolila, J.M. Tsay, S. Doose, J.J. Li, G. Sundaresan, A.M. Wu, S.S. Gambhir, S. Weiss, Quantum dots for live cells, in vivo imaging, and diagnostics, Science 307 (2005) 538–544.
[5] A.M. Derfus, W.C.W. Chan, S.N. Bhatia, Probing the cytotoxicity of semiconductor quantum dots, Nano Lett. 4 (2004) 11–18.
[6] C. Kirchner, T. Liedl, S. Kudera, T. Pellegrino, A. Munoz Javier, H.E. Gaud, S. Stölzle, N. Fertig, W.J. Parak, Cytotoxicity of colloidal CdSe and CdSe/ZnS nanoparticles, Nano Lett. 5 (2005) 331–338.
[7] N. Chen, Y. He, Y. Su, X. Li, Q. Huang, H. Wang, X. Zheng, R. Tai, C. Fan, The cytotoxicity of cadmium-based quantum dots, Biomaterials 33 (2012) 1238–1244.
[8] W. Liu, S. Zhang, L. Wang, C. Qu, C. Zhang, L. Hong, L. Yuan, Z. Huang, Z. Wang, S. Liu, G. Jiang, CdSe quantum dots (QD)-induced morphological and functional impairments to liver in mice, PLoS ONE 6 (2011) e24406.
[9] Y. Su, Y. He, H. Lu, L. Sai, Q. Li, W. Li, L. Wang, P. Shen, Q. Huang, C. Fan, The cytotoxicity of cadmium based, aqueous phase—synthesized, quantum dots and its modulation by surface coating, Biomaterials 30 (2009) 19–25.
[10] Y. Su, M. Hu, C. Fan, Y. He, Q. Li, W. Li, L.-H. Wang, P. Shen, Q. Huang, The cytotoxicity of CdTe quantum dots and the relative contributions from released cadmium ions and nanoparticle properties, Biomaterials 31 (2010) 4829–4834.
[11] R.A. Hardman, A toxicologic review of quantum dots: toxicity depends on physicochemical and environmental factors, Environ. Health Perspect. 114 (2006) 165–172.
[12] A. Hoshino, K. Fujioka, T. Oku, M. Suga, Y.F. Sasaki, T. Ohta, M. Yasuhara, K. Suzuki, K. Yamamoto, Physicochemical properties and cellular toxicity of nanocrystal quantum dots depend on their surface modification, Nano Lett. 4 (2004) 2163–2169.
[13] Y. Tang, S. Han, H. Liu, X. Chen, L. Huang, X. Li, J. Zhang, The role of surface chemistry in determining in vivo biodistribution and toxicity of CdSe/ZnS core–shell quantum dots, Biomaterials 34 (2013) 8741–8755.
[14] A. Aboulaich, C.-M. Tilmaciu, C. Merlin, C. Mercier, H. Guilloteau, G. Medjahdi, R. Schneider, Physicochemical properties and cellular toxicity of (poly)aminoalkoxysilanes-functionalized ZnO quantum dots, Nanotechnology 23 (335101) (2012) 9.
[15] A. Shiohara, A. Hoshino, K. Hanaki, K. Suzuki, K. Yamamoto, On the cyto-toxicity caused by quantum dots, Microbiol. Immunol. 48 (2004) 669–675.
[16] R. Schneider, C. Wolpert, H. Guilloteau, L. Balan, J. Lambert, C. Merlin, Exposure of bacteria to CdTe quantum dots: the importance of surface chemistry on cytotoxicity, Nanotechnology 20 (225101) (2009) 10.
[17] J.H. Priester, P.K. Stoimenov, R.E. Mielke, S.M. Webb, C. Ehrhardt, J.P. Zhang, G.D. Stucky, P.A. Holden, Effects of soluble cadmium salts versus CdSe quantum dots on the growth of planktonic *Pseudomonas aeruginosa*, Environ. Sci. Technol. 43 (2009) 2589–2594.
[18] A.P. Alivisatos, W. Gu, C. Larabell, Quantum dots as cellular probes, Annu. Rev. Biomed. Eng. 7 (2005) 55–76.
[19] J. Kim, Y. Park, T.H. Yoon, C.S. Yoon, K. Choi, Phototoxicity of CdSe/ZnSe quantum dots with surface coatings of 3-mercaptopropionic acid or tri-n-octylphosphine oxide/gum arabic in *Daphnia magna* under environmentally relevant UV-B light, Aquat. Toxicol. 97 (2010) 116–124.
[20] S.J. Cho, D. Maysinger, M. Jain, B. Röder, S. Hackbarth, F.M. Winnik, Long-term exposure to CdTe quantum dots causes functional impairments in live cells, Langmuir 23 (2007) 1974–1980.
[21] D.R. Cooper, N.M. Dimitrijevic, J.L. Nadeau, Photosensitization of CdSe/ZnS QDs and reliability of assays for reactive oxygen species production, Nanoscale 2 (2010) 114–121.
[22] C.B. Murray, D.J. Norris, M.G. Bawendi, Synthesis and characterization of nearly monodisperse CdE (E = sulfur, selenium, tellurium) semiconductor nanocrystallites, J. Am. Chem. Soc. 115 (1993) 8706–8715.
[23] Z.A. Peng, X.G. Peng, Formation of high-quality CdTe, CdSe, and CdS nanocrystals using CdO as precursor, J. Am. Chem. Soc. 123 (2001) 183–184.
[24] L. Qu, X. Peng, Control of photoluminescence properties of CdSe nanocrystals in growth, J. Am. Chem. Soc. 124 (2002) 2049–2055.
[25] S.F. Wuister, I. Swart, F.V. Driel, S.G. Hickey, C.D.M. Donega, Highly luminescent water-soluble CdTe quantum dots, Nano Lett. 3 (2003) 503–507.
[26] R. Schneider, L. Balan, Hydrothermal routes for the synthesis of CdSe core quantum dots, in: A. Al-Ahmadi (Ed.), State-of-the-Art of Quantum Dot System Fabrications, InTech, Rijeka, Croatia, 2012.
[27] A. Aboulaich, D. Billaud, M. Abyan, L. Balan, J.-J. Gaumet, G. Medjahdi, R. Schneider, One-pot noninjection route to CdS quantum dots via hydrothermal synthesis, ACS Appl. Mater. Interfaces 4 (2012) 2561–2569.
[28] F. Aldeek, C. Mustin, L. Balan, G. Medjahdi, T. Roques-Carmes, P. Arnoux, R. Schneider, Enhanced photostability from CdSe(S)/ZnO core/shell quantum dots and their use in bio-labelling, Eur. J. Inorg. Chem. (2011) 794–801.
[29] F. Aldeek, L. Balan, G. Medjahdi, T. Roques-Carmes, J.-P. Malval, C. Mustin, J. Ghanbaja, R. Schneider, Enhanced optical properties of core/shell/shell CdTe/CdS/ZnO quantum dots prepared in aqueous solution, J. Phys. Chem. C 113 (2009) 19458–19467.
[30] D.L. Klayman, T.S. Griffin, Reaction of selenium with sodium borohydride in protic solvent. A facile method for the introduction of selenium into organic molecules, J. Am. Chem. Soc. 95 (1973) 197–199.
[31] S. Chen, X. Zhang, Q. Zhang, X. Hou, Q. Zhou, J. Yan, W. Tan, CdSe quantum dots decorated by mercaptosuccinic acid as fluorescent probe for Cu2+, J. Lumin. 131 (2011) 947–951.
[32] M. Grabolle, M. Spieles, V. Lesnyak, N. Gaponik, A. Eychmüller, U. Resch-Genger, Determination of the fluorescence quantum yield of quantum dots: suitable procedures and achievable uncertainties, Anal. Chem. 81 (2009) 6285–6294.
[33] W.W. Yu, L.H. Qu, W.Z. Guo, X.G. Peng, Experimental determination of the extinction coefficient of CdTe, CdSe, and CdS nanocrystals, Chem. Mater. 15 (2003) 2854–2860.
[34] A. Anas, H. Akita, H. Harashima, T. Itoh, M. Ishikawa, V. Biju, Photosensitized breakage and damage of DNA by CdSe–ZnS quantum dots, J. Phys. Chem. B 112 (2008) 10005–10011.
[35] X. Fang, G. Mark, C. von Sonntag, OH radical formation by ultrasound in aqueous solutions. Part I. The chemistry underlying the terephthalate dosimeter, Ultrason. Sonochem. 3 (1996) 57–63.

[36] T.J. Mason, J.P. Lorimer, D.M. Bates, Y. Zhao, Dosimetry in sonochemistry: the use of aqueous terephthalate ion as a fluorescent monitor, Ultrason. Sonochem. 1 (1994) S91–S95.
[37] P. Corbisier, D. van der Lelie, B. Borremans, A. Provoost, V. de Lorenzo, N.L. Brown, J.R. Loyd, J.L. Hobamn, E. Csöregi, G. Johansson, B. Mattiasson, Whole cell- and protein-based biosensors for the detection of bioavailable heavy metals in environmental samples, Anal. Chim. Acta 387 (1999) 235–244.
[38] A. Zaslaver, A. Bren, M. Ronen, S. Itzkovitz, I. Kikoin, S. Shavit, W. Liebermeister, M.G. Surette, U. Alon, A comprehensive library of fluorescent transcriptional reporters for *Escherichia coli*, Nat. Methods 3 (2006) 623–628.
[39] L. Xu, K. Chen, H.M. El-Khair, M. Li, X. Huang, Enhancement of band-edge luminescence and photo-stability in colloidal CdSe quantum dots by various surface passivation technologies, Appl. Surf. Sci. 172 (2001) 84–88.
[40] W.R. Algar, U.J. Krull, Luminescence and stability of aqueous thioalkyl acid capped CdSe/ZnS quantum dots correlated to ligand ionization, ChemPhysChem 8 (2007) 561–568.
[41] H. Zhang, Z. Zhou, B. Yang, M. Gao, The influence of carboxyl groups on the photoluminescence of mercaptocarboxylic acid-stabilized CdTe nanoparticles, J. Phys. Chem. B 107 (2003) 8–13.
[42] Y. Li, W. Zhang, J. Niu, Y. Chen, Mechanism of photogenerated reactive oxygen species and correlation with the antibacterial properties of engineered metal-oxide nanoparticles, ACS Nano 6 (2012) 5164–5173.
[43] B.I. Ipe, M. Lehnig, C.M. Niemeyer, On the generation of free radical species from quantum dots, Small 1 (2005) 706–709.
[44] C. Bohne, K. Faulhaber, B. Giese, A. Hafner, A. Hofmann, H. Ihmels, A.-K. Kohler, S. Pera, F. Schneider, M.A.L. Sheepwash, Studies on the mechanism of the photo-induced DAN damage in the presence of acridizinium salts involvement of singlet oxygen and an unusual source for hydroxyl radicals, J. Am. Chem. Soc. 127 (2005) 76–85.
[45] Y. Iida, K. Yasui, T. Tuziuti, M. Sivakumar, Y. Endo, Ultrasonic cavitation in microspace, Chem. Commun. (2004) 2280–2281.
[46] H. Sies, Oxidative stress: oxidants and antioxydants, Exp. Physiol. 82 (1997) 291–295.